Published in final edited form as:
Am J Transplant. 2015 January ; 15(1): 64–75. doi:10.1111/ajt.12999.

Optimization and critical evaluation of decellularization strategies to develop renal extracellular matrix scaffolds as biological templates for organ engineering and transplantation

Mireia Caralt, M.D., Ph.D.[1,2,3], **Joseph S. Uzarski, Ph.D.**[1,2], **Stanca Iacob, M.D., Ph.D.**[1,2], **Kyle P. Obergfell, B.S.**[1], **Natasha Berg, M.D.**[4], **Brent M. Bijonowski, M.Sc.**[1,2], **Kathryn M. Kiefer, M.Sc.**[1], **Heather H. Ward, Ph.D.**[5], **Angela Wandinger-Ness, Ph.D.**[6], **William M. Miller, Ph.D.**[7,8], **Zheng J. Zhang, M.D.**[1,2], **Michael M. Abecassis, M.D., MBA**[1,2], and **Jason A. Wertheim, M.D., Ph.D.**[1,2,8,9,10,11,*]

[1]Comprehensive Transplant Center, Feinberg School of Medicine, Northwestern University, Chicago, IL, 60611

[2]Department of Surgery, Northwestern University Feinberg School of Medicine, Chicago, IL, 60611

[3]Servei Cirurgia HepatoBilioPancreatica i Trasplantaments. Hospital Universitari Vall Hebron. Universitat Autonoma de Barcelona. Spain

[4]Department of Pathology, Northwestern University Feinberg School of Medicine, Chicago, IL, 60611

[5]Department of Internal Medicine, University of New Mexico, Albuquerque, NM, 87131

[6]Department of Pathology, University of New Mexico, Albuquerque, NM, 87131

[7]Department of Chemical and Biological Engineering, Northwestern University, Evanston, IL, 60201

[8]Chemistry of Life Processes Institute, Northwestern University, Evanston, IL, 60201

[9]Department of Surgery, Jesse Brown VA Medical Center, Chicago, IL, 60612

[10]Institute for BioNanotechnology in Medicine, Northwestern University, Chicago, IL, 60611

[11]Department of Biomedical Engineering, Northwestern University, Evanston, IL, 60201

Abstract

The ability to generate patient-specific cells through induced pluripotent stem cell (iPSC) technology has encouraged development of three-dimensional extracellular matrix (ECM)

[*]**Address for correspondence:** Jason A. Wertheim, M.D., Ph.D., 676 St. Clair St. Suite 1900, Chicago, Illinois 60611, Telephone: (312) 695-0257, Fax: (312) 503-3366, jwerthei@nmh.org.

DISCLOSURE:
The authors of this manuscript have no conflicts of interest to disclose as described by the American Journal of Transplantation.

SUPPORTING INFORMATION:
Additional Supporting Information may be found in the online version of this article.
Supplementary Materials and Methods

scaffolds as bioactive substrates for cell differentiation with the long-range goal of bioengineering organs for transplantation. Perfusion decellularization uses the vasculature to remove resident cells, leaving an intact ECM template wherein new cells grow; however, a rigorous evaluative framework assessing ECM structural and biochemical quality is lacking. To address this, we developed histologic scoring systems to quantify fundamental characteristics of decellularized rodent kidneys: ECM structure (tubules, vessels, glomeruli) and cell removal. We also assessed growth factor retention—indicating matrix biofunctionality. These scoring systems evaluated three strategies developed to decellularize kidneys (1% Triton X-100, 1% Triton X-100/0.1% sodium dodecyl sulfate (SDS), and 0.02% Trypsin-0.05% EGTA/1% Triton X-100). Triton and Triton/SDS preserved renal microarchitecture and retained matrix-bound bFGF and VEGF. Trypsin caused structural deterioration and growth factor loss. Triton/SDS-decellularized scaffolds maintained three hours of leak-free blood flow in a rodent transplantation model and supported repopulation with human iPSC-derived endothelial cells and tubular epithelial cells *ex vivo*. Taken together, we identify an optimal Triton/SDS-based decellularization strategy that produces a biomatrix that may ultimately serve as a rodent model for kidney bioengineering.

INTRODUCTION

One approach to address donor organ shortage is stem cell and organ engineering, which have played increasing roles in tissue and organ transplantation research (1). Decellularization is the process by which allogeneic or xenogeneic cells are extracted from immunologically incompatible tissues or organs to produce an acellular, bioactive extracellular matrix (ECM) that is directly implanted (e.g., cell-free biological scaffolds for surgical hernia repair) or used as a template scaffold to grow cells for engineering complex tissues or organs (2, 3). Using stem cell technology, primary cells may one-day be isolated from patients in need of an organ transplant, expanded *in vitro*, and seeded onto decellularized matrices to produce a compatible, functional organ on demand (4). Scaffolds for bioengineering should retain many of the natural structural and cell-signaling features of the original tissue and act as bioactive three-dimensional (3D) templates to guide repopulating cells. The importance of matrix biofunctionality has been demonstrated in the lung where alveolar epithelial cells, developed from human induced pluripotent stem cells (iPSCs), further matured into type I pneumocytes on decellularized human or rodent lung parenchyma (5). In the clinical setting, implantation of bioengineered tissues using autologous cells has led to promising, though preliminary, results in several case studies (e.g., trachea (6), bladder (7), blood vessels (8)), providing a pathway for clinical translation of a wider array of tissue engineering technologies.

The ECM plays a critical role in presenting both a structural architecture and biochemical milieu to patient-specific cells, stressing the importance of developing a quantitative assessment of matrix scaffold integrity. A variety of techniques have been reported for tissue decellularization in general (reviewed in 1, 9), and kidney in particular (reviewed in (10)), but a standardized method to compare decellularization procedures is lacking. Perfusion of chemical or enzymatic reagents through the native vasculature makes it possible to derive acellular ECM scaffolds from whole organs, including heart (11), lung (12), liver (13), and kidney (14–16). However, due to variations in size, composition, and structural properties,

the decellularization process warrants careful optimization in an organ-specific manner with special attention to retaining key components of the ECM.

In an important proof-of-concept study establishing the feasibility of kidney bioengineering, the Ott group reported a 5-day decellularization strategy that upon repopulation with rat neonatal kidney cells and human umbilical vein endothelial cells led to partial restoration of renal filtration and reabsorption (9, 16). Given the context of these and other (17–19) promising findings that suggest a central role for ECM in stem/progenitor cell differentiation, we developed a standardized assessment of the structural and biochemical repertoire of renal ECM as a basis to further understand cell-ECM interactions on the structural and molecular level. In this report, we focus on rodent scaffolds, in lieu of large animal models, because their smaller size is conducive to cell repopulation with the limited yield, differentiation efficiency, and availability of stem/progenitor cells through current stem cell technology. Herein, we present a quantitative comparison of three, short (~26h) decellularization procedures evaluated by histologic scoring systems that weigh both efficiency of cellular removal and retention of matrix integrity across a spectrum of optimized decellularization strategies and point to an ideal matrix composition that supports *in vivo* implantation into a rodent model and *ex vivo* cellular repopulation with human renal tubular epithelial cells and iPSC-derived endothelial cells. Furthermore, we show, in a process-dependent manner, that scaffolds retain growth factors involved in known pathways of embryologic (vascular endothelial growth factor (VEGF)) and directed (basic fibroblast growth factor (bFGF)) differentiation of stem/progenitor cells toward a mature renal phenotype.

MATERIALS AND METHODS

Kidney recovery

Male Sprague Dawley rats (250–300 g) were used to supply kidneys (see Supporting Information for additional methods). All procedures involving animals were performed according to guidelines approved by the Institutional Animal Care and Use Committee of Northwestern University.

Decellularization

Each kidney was perfused with decellularization solutions through a cannula placed into the renal artery and attached to a peristaltic pump; volume and duration of each agent is noted (Figure 1A).

Histologic scoring

Each decellularization strategy was evaluated by a pathologist (N.B.) blinded to each protocol and graded against a five-point scale for nuclear basophilia (degree of cellular loss) and architecture after staining with hematoxylin & eosin (H&E). Each scale was evaluated for glomeruli, tubules, and blood vessels in 5–10 high-powered (40×) fields per histologic section for each kidney (n=5–7 per protocol). Nuclear basophilia was scored: 1 (optimal score) complete loss of nuclear basophilia (100% cellular removal); 2 substantial loss (70%); 3 moderate loss (50%); 4 minimal loss (30%); 5 no loss of nuclear basophilia (0%).

Architectural preservation was scored: 1 lowest value (no outlines visible, marked disruption/breakdown of tissue); 2 marked disruption (outlines visible/marked disruption); 3 moderate disruption (outlines visible/moderate disruption); 4 minimal disruption (outlines visible/minimal disruption); 5 essentially normal tissue architecture (outlines visible, architecture intact), the goal for any decellularization strategy.

DNA quantification

Kidneys were cut into small pieces and digested using Proteinase K (Promega # V3021) for 48h at 37°C. DNA was extracted as described (13). DNA was quantified spectrophotometrically using NanoDrop technology. The assay was performed on five normal kidneys and three kidneys per group.

Growth factor evaluation

Growth factors were isolated from kidneys as described (13). Concentrations of bFGF and VEGF were determined with the Quantikine human FGF basic immunoassay (R&D Systems # DFB50) and Quantikine rat VEGF immunoassay (R&D Systems # RRV00). Assays were performed in duplicate for each of three kidneys per group. The amount of remaining growth factor was normalized to the initial dry-weight of control kidneys to allow for comparison across all conditions.

Transplantation of acellular scaffold

A right nephrectomy was performed on a recipient Sprague Dawley rat, and the acellular scaffold was implanted. Two hundred units of heparin were injected through the penile vein. An end-to-side anastomosis with 10/0 suture was performed between the aorta of the scaffold and the aorta of the recipient, and between the renal vein of the scaffold and the inferior vena cava of the recipient.

Recellularization of whole-organ, acellular scaffolds with iPSC-derived endothelial cells

Purified human endothelial cells derived from iPSCs (Cellular Dynamics International, Inc. Madison, WI) and labeled with CellTrace™ CFSE Cell Proliferation Kit (Molecular Probes #C34554), were injected slowly by hand through the renal artery (5×10^6 cells). The seeded scaffold was placed in a Petri dish with maintenance medium. After 36h at 37°C, the seeded scaffold was cut into 1-mm slices and visualized using a Nikon AZ-100 fluorescence microscope.

Recellularization of whole-organ scaffolds in a custom bioreactor

We designed a perfusion-based bioreactor constructed from two glass flanges placed end-to-end, with a valve and septum for media sampling similar to that shown in Figure 2 of (20). Immortalized human renal cortical tubular epithelial (RCTE) cells (21, 22) (40×10^6 cells in 2 mL) were infused through the bioreactor tubing and anterograde pulsatile perfusion began immediately through the renal artery at 25 mL/min (232 mmHg) for 15 min before decreasing the flow rate to 4 mL/min up to seven days. DMEM/F12 medium (Life Technologies #11320–082) supplemented with 10% FBS and 1× penicillin/streptomycin was changed 24h after seeding and then every 48h.

Statistical analyses

Statistical analyses were performed using SPSS software with one-way analysis of variance (ANOVA) followed by post-hoc Tukey's Honest Significant Difference (HSD) test for pairwise comparison of means and statistical significance was set at $p<0.05$.

RESULTS

Evaluation of decellularized kidneys reveals cellular loss and retention of the innate microscopic structure

Rat kidneys were decellularized by perfusion through the renal artery using one of three strategies: 1% Triton X-100 alone (Triton), sequential perfusion of 1% Triton X-100/0.1% SDS (Triton/SDS), or sequential perfusion of 0.02% trypsin-0.05% EGTA/1% Triton X-100 (Trypsin-EGTA/Triton; Figure 1 A). Kidneys decellularized using Triton alone retained their parenchymal color (Figure 1 B). Both Triton/SDS and Trypsin-EGTA/Triton led to a translucent appearance with gross preservation of the underlying vasculature.

Microscopic assessment by H&E staining of decellularized kidneys mirrored the macroscopic evaluation. Large empty spaces, once occupied by cells, could be seen using Triton/SDS or Trypsin-EGTA/Triton (Figure 2). In contrast, Triton X-100 alone was ineffective at removing endothelial and smooth muscle cells from vessels and mesangial cells from glomeruli. Trypsin-EGTA/Triton was effective at removing cells, but left proteinaceous debris within the matrix.

For all protocols, microarchitecture of primary, functional components of the kidney (tubules, glomeruli, and vessels) was generally well preserved and similar to that of native kidneys as revealed by SEM (Figure 3). A honeycomb-like appearance with retention of ECM between individual tubules was visualized at low magnification using either Triton/SDS or Trypsin-EGTA/Triton. Both strategies preserved glomerular basement membrane architecture with mesangial cell removal, as shown at high magnification (Figure 3 F, H).

Establishment of semi-quantitative, pathology-based grading scales for kidney decellularization

We developed two semi-quantitative grading scales to provide a consistent standard and to institute a quality measurement of organ architecture going forward. In so doing, we evaluated the ability to differentiate the effectiveness of our three decellularization strategies to achieve the tight balance between 1) effective cell removal and 2) retention of native ECM architecture. A pathologist performed a blinded scoring of 5–10 H&E-stained sections of each decellularized kidney for nuclear basophilia (e.g., cell removal, optimal score 1, n=5–7, Figure 4) and preservation of matrix architecture (optimal score 5, n=5–7, Figure 5). Representative histologic images for each score are shown (Supporting Figure 1). Triton decellularization resulted in substantial loss (~70%) of nuclear basophilia in renal tubules (average score 1.9±0.9, $p<0.001$) and glomeruli (average score 2.1±0.4, $p<0.001$), but only minimal to moderate (30–50%) loss of nuclei in blood vessels (score 3.4±0.8, $p=0.001$; Figure 4) compared to native, untreated kidneys. In contrast, Triton/SDS resulted in

complete cell removal (average score 1.0±0.0) from all three components of the renal ECM; Trypsin-EGTA/Triton resulted in an average score of 1.3±0.8 for vessels, 1.1±0.4 for glomeruli, and 1.1±0.4 for tubules ($p<0.001$ for both methods compared to native kidneys for all components). Though Triton/SDS resulted in more consistent, complete cell removal compared to Trypsin-EGTA/Triton, the difference did not reach statistical significance (Supporting Table 1). We also quantified residual DNA remaining in decellularized kidneys as a further surrogate marker for cell removal. DNA content (as a percentage of native kidneys) of Triton/SDS-treated kidney scaffolds (median 3.08%, range 1.73–7.50%) was significantly lower than those treated with Triton alone (median 89.14%, range 74.81–98.61%, $p<0.001$) or Trypsin-EGTA/Triton (median 22.47%, range 19.02–24.39%, $p<0.001$). Triton/SDS removed an average of ~95% of native DNA, a benchmark indicating effective cell removal comparable to other organs such as liver (23).

Using the semi-quantitative scoring system, less dramatic differences were found in scaffold architecture. All methods retained vessel integrity (average score 5.0; Figure 5 D), while scores for glomeruli and tubules ranged from ~4 to ~5 (Figure 5 B,C). The only significant evidence for matrix deterioration was within glomeruli of Trypsin-EGTA/Triton (average score 3.9±0.7, $p=0.009$, Figure 5 C) or Triton/SDS (average score 4.0±0.6, $p=0.031$) decellularized kidneys.

Structural proteins and ECM-bound growth factors are retained after decellularization

As a prelude to utilizing decellularized scaffolds as a 3D matrix to grow cells, we next evaluated retention of specific structural proteins and growth factors following decellularization as both are critical to the bioactivity of renal matrix and initiate outside-in signaling leading to cell differentiation and proliferation. Native and decellularized kidneys were stained for type IV collagen, the most abundant component of the kidney ECM, or laminin, an important component of the basement membrane that supports tubule formation and kidney development (24). Though some loss of collagen IV was expected, and identified across all strategies given the tight balance between cell removal and matrix preservation, Triton/SDS resulted in the smallest loss of collagen IV staining, noted predominantly within the glomeruli (Figure 6 A–D) and along the kidney capsule (not shown) with less surrounding renal tubules. Only Triton/SDS-processed scaffolds lacked DAPI staining, indicating complete removal of cells and nuclear debris, in agreement with our assessment of DNA content and basophilia score. Similar to collagen IV, there was some loss of laminin using all strategies (Figure 6 E–H), though Triton yielded the greatest retention in this case.

Various isoforms of the FGF receptor have been identified in the developing kidney and are important for early renal patterning and directed differentiation of iPSCs toward a renal cell fate (25, 26). There was no significant difference in bFGF retention between Triton and Triton/SDS-decellularized kidneys (Figure 7 A, $p=0.983$), and kidneys decellularized using either protocol retained roughly 30% of the bFGF, which is similar in absolute amount and degree of retention in decellularized liver (13), adipose tissue (27), and mesothelium (28). bFGF was undetectable in Trypsin-EGTA/Triton decellularized kidneys. VEGF, important for angiogenesis and renal podocyte development (29, 30), was retained at minimal concentrations in these scaffolds, but was found at a higher, though not significantly

different, level in Triton and Triton/SDS decellularized kidneys (Figure 7 B, ANOVA; p=0.166).

Decellularized kidneys retain a patent vasculature and are transplantable

Based on the analysis just described, we determined Triton/SDS to be the most efficacious strategy balancing cell removal and maintenance of both architecture and molecular components of the renal ECM (Table 1). Thus, we continued our assessment using this strategy to evaluate integrity of the renal vasculature to support blood flow and cell growth in subsequent experiments. We perfused red or blue polymers through the renal artery or vein, respectively, to produce a cast of the vasculature, which demonstrates even the tiniest terminal branch-points of the renal vascular network remain intact (Figure 8 A). Preservation of the intricate branching pattern was also apparent under bright-field microscopy (Figure 8 B).

To further evaluate matrix retention, and determine if structural integrity was sufficient as a scaffold for a future implantable, bioengineered kidney, we investigated its ability to hold suture and support systemic arterial blood flow by implanting a whole, Triton/SDS decellularized scaffold into a Sprague Dawley recipient in an orthotopic position. The decellularized renal artery and vein were easily anastomosed to the recipient aorta and vena cava, respectively. There was no sign of clotting or major bleeding at the anastomoses, kidney capsule, or anywhere within the scaffold at 30 minutes after reperfusion (Figure 8 C–D), through there was generalized soft tissue oozing at later time-points due to systemic heparinization. Nonetheless, kidney scaffolds remained intact *in situ* for up to three hours until the animal was sacrificed.

Decellularized kidney scaffolds support repopulation by human endothelial and tubular epithelial cells

To confirm that decellularized matrices support recellularization, we seeded Triton/SDS-processed whole-organ scaffolds with either iPSC-derived endothelial cells or an immortalized human RCTE cell line. iPSC-derived endothelial cells stained with CFSE could clearly be seen outlining branching vasculature and abutting what appear to be individual glomeruli (Figure 8 E–F). RCTE cells were infused into whole-organ scaffolds through the renal artery in a specialized bioreactor (Figure 9 A). At 24h post-seeding, RCTE cells formed what appear to be tubular structures that coalesced over time (Figure 9 A). Importantly, even though RCTE cells were injected through the arterial network, they were not found within arterioles (Figure 9 A, Elastin), suggesting cells translocated into the parenchyma or peri-tubular space to rest on the basement membrane (Figure 9 A, PAS).

As a quantitative index for recellularization, we used image threshold analysis to determine the degree of early cell adhesion to whole-kidney scaffolds. Twenty-four hours after infusion of RCTE cells, 50.5% of the renal area (cells+ECM) was recellularized (Figure 9B). These repopulating cells then displayed a time-dependent increase in metabolic activity by resazurin reduction ($p<0.05$), suggesting persistent cell viability and proliferation within the scaffold (Figure 9B). Glucose consumption declined initially ($p<0.001$) and remained constant through the end of the seven-day experiment. Lactate production increased during

the first five days within the bioreactor (p=0.004, Figure 9C). Taken together, decreasing glucose consumption and increasing lactate production indicates an increasing yield of lactate from glucose, suggesting increased reliance on glycolysis. The peak apparent yield (~1.5 mol lactate/mol glucose) remained below the theoretical maximum of 2.0, suggesting partial oxidative metabolism of glucose. However, it is likely that some portions of the repopulated scaffold were oxygen-limited, and we plan to evaluate the influence of perfusion rate on metabolism in future experiments. Importantly, we did not see evidence of necrosis, indicative of cell death, in histologic sections during this evaluation (Figure 9A). Together, these experiments demonstrate that appropriate decellularization can produce acellular kidney scaffolds that support cellular adhesion, distribution, and metabolic activity within a whole-organ 3D biomatrix.

DISCUSSION

A high degree of enthusiasm for the development of bioengineered organs and tissues exists within the transplantation community based on the promise of early clinical success implanting autologous cell-seeded artificial bladders in 2006 (7) and transplantation of a decellularized cadaveric trachea in 2008 (6). More recently, clinical evaluation of tissue engineered nasal cartilage (31) and genitourinary tubular tissues (32, 33) were evaluated in small, first-in-human trials. Bioengineering solid organs for transplantation has been far more challenging than two-dimensional planar tissues, due to the structural complexity and need for a vascular network to supply nutrients to deeper regions of thick organs. Since the first report describing perfusion of detergents through the coronary arteries of rodent hearts by Ott and Taylor in 2008 (11), several approaches to remove cells from the heart (34), liver (13, 23, 35) and lung (12, 36) have been described. Likewise, a variety of perfusion decellularization protocols for kidney have been tested for rodents, pigs, and humans (reviewed in 10 and described in 14–16, 18, 19, 37, 38), but few studies report data specifically comparing the influence of different chemical-based decellularization procedures on resulting ECM architecture and sufficiency for supporting recellularization (14, 39).

Herein, we present an in-depth comparison of three optimized and diverse, short (26h) decellularization strategies based on a non-ionic detergent (Triton) alone, or in combination with an ionic detergent (SDS) or an enzyme solution (Trypsin). Unique to our approach in the rodent kidney, we provide focused, quantitative biochemical and structural analyses of cell removal and maintenance of appropriate ECM composition, microstructure, and growth factors for the development of a bioactive matrix capable of recellularization. Importantly, we show that the decellularization strategy greatly affects the degree of cell removal, presence of residual DNA, and preservation of growth factors important for renal development.

The challenge to developing cell-free matrix scaffolds through decellularization is the narrow balance between effective cell removal and maintenance of the natural, biochemical milieu of the native tissue architecture to the highest degree possible (Table 1). Removal of the cellular content is essential due to the adverse immune responses elicited by allogeneic or xenogeneic cell membrane epitopes, DNA and damage-associated molecular pattern

molecules (40–42). In our study, kidneys decellularized with 1% Triton alone contained residual cells within glomeruli, tubules, and vessels. Consistent with this finding, we found higher residual DNA than those processed using Triton in conjunction with SDS or Trypsin-EGTA. To place these findings in the larger context of inter-species variability, Nakayama et al. found residual cell debris and nuclei in kidneys from rhesus monkeys after 1% Triton, but also noted disruption of the basement membrane with loss of glomerular ECM organization (39). Sullivan et al. (14) and Orlando et al. (15) reported incomplete decellularization of porcine kidneys using Triton alone or with ammonium hydroxide, suggesting that the unique renal anatomy (with cells located inside a very dense and tortuous ECM architecture) may explain the lower efficiency of Triton in decellularizing kidneys compared to other tissues (e.g., liver (23), heart valve (3)).

SDS has been abandoned as a decellularizing agent in some organs, such as liver, because of its damaging effects on ECM (13, 23, 43). Taking this into consideration, we perfused a low concentration (0.1%) of SDS following Triton and found that it achieved superior cell removal. We observed that kidneys became transparent immediately following perfusion of SDS, with removal of ~95% residual DNA. Unlike other reports implicating SDS in matrix disruption, our blinded scoring of H&E-stained kidney sections reveals little to no damage in renal tubules and vessels and minimal disruption of glomeruli, though we show some loss of laminin and collagen IV, illustrating the tight balance decellularization strategies must achieve (9). The disparity between efficiency of decellularization strategies in liver and kidney is an important insight into the field of organ engineering, and underscores tissue heterogeneity between organs (and possibly species). Trypsin-based decellularization strategies may be optimal for liver with a porous, fenestrated endothelium (13), but, as we present here, are not effective in the dense structure of the kidney and lead to growth factor loss.

ECM-bound growth factors facilitate cell trafficking, proliferation, and differentiation. In addition to its established role in promoting endothelial cell proliferation and angiogenesis, VEGF is critical for renal podocyte development (29, 30) and formation of functional glomerular filtration barriers (44). Importantly, we demonstrate retention of growth factors (bFGF and VEGF) within the kidney biomatrix after decellularization. This finding is bolstered by the observation of Orlando et al. who demonstrated that acellular human renal ECM induced angiogenesis in the chicken chorioallontoic membrane even with a stronger 0.5% SDS decellularization method (38). However, as an example of the delicate balance, Nakayama et al. did not detect bFGF in rhesus monkey kidneys using the higher concentration of 1% SDS (45). Similar to our findings in which trypsin led to low levels of VEGF, Soto-Gutierrez et al. did not detect VEGF in rodent livers decellularized using a similar protocol (13) and Hoganson et al. detected minimal to no VEGF in commercially available decellularized small intestinal submucosa (28) but did find FGF, as have others (46). Collectively, our results suggest careful use of detergent-based decellularization protocols in the kidney may be more appropriate than trypsin to preserve ECM-based growth factors.

As a prelude to future organ bioengineering using our Triton/SDS strategy, we show that the native vascular network remains intact and well-preserved throughout this process and can

be easily transplanted into a rodent model. Moreover, in contrast to other recent reports, we demonstrate a new method to deliver renal epithelial cells to the scaffold through the renal artery at high pressure that achieves equivalent or improved results compared to others using ureteral (16) or low-pressure arterial infusion (19). Significantly, even though our scaffolds were developed using a relatively short (26h) decellularization procedure and exposure to solutions that disrupt cellular integrity, we demonstrate that this strategy does not present deleterious effects for subsequent cell repopulation as 1) human iPSC-derived endothelial cells repopulated the vasculature and 2) renal cortical tubular epithelial cells infused under high pressure translocated out of the arterial circulation into peri-tubular structures. RCTE cells infused in this manner led to ~50% recellularization at 24 hours and form what appear to be tubules with increasing metabolic activity. Taken together, we have identified an optimized decellularization strategy using Triton/SDS as an effective, time-efficient strategy to develop whole-kidney ECM scaffolds which, coupled with a quantitative quality assessment, can be used as a structural foundation for the development of kidney tissue engineering-based therapies.

Supplementary Material

Refer to Web version on PubMed Central for supplementary material.

ACKNOWLEDGMENTS

We thank Dr. Joseph Kang (Department of Preventative Medicine and Comprehensive Transplant Center, Northwestern University) for his helpful consultation on statistical analysis. We thank the support of the Zell Family Foundation, the Excellence in Academic Medicine Act through the Illinois Department of Healthcare and Family Services, Northwestern Memorial Foundation Dixon Translational Research Grants Initiative, and the American Society of Transplant Surgeon's Faculty Development Grant to J.A.W. We thank support from NIDDK R01 DK050141 to A.W.N. and NIGMS K12 GM088021 and reserve funds from Dialysis Clinic, Inc. to H.H.W. We thank Cellular Dynamics International for supplying iCell endothelial cells. This work was supported by the Northwestern University Mouse Histology and Phenotyping Laboratory and a Cancer Center Support Grant (NCI CA060553). Imaging work was performed at the Northwestern University Cell Imaging Facility generously supported by NCI CCSG P30 CA060553 awarded to the Robert H Lurie Comprehensive Cancer Center.

Abbreviations

bFGF	basic fibroblast growth factor
CFSE	carboxyfluorescein diacetate succinimidyl ester
ECM	extracellular matrix
H&E	hematoxylin and eosin
iPSC	induced pluripotent stem cell
PAS	periodic acid-Schiff
RCTE	renal cortical tubular epithelial
SEM	scanning electron microscopy
SDS	sodium dodecyl sulfate
WRF	Weigert's resorcin-fuchsin

REFERENCES

1. Badylak SF, Taylor D, Uygun K. Whole-organ tissue engineering: decellularization and recellularization of three-dimensional matrix scaffolds. Annu Rev Biomed Eng. 2011; 13:27–53. [PubMed: 21417722]
2. Gilbert TW, Sellaro TL, Badylak SF. Decellularization of tissues and organs. Biomaterials. 2006; 27(19):3675–3683. [PubMed: 16519932]
3. Rieder E, Kasimir MT, Silberhumer G, Seebacher G, Wolner E, Simon P, et al. Decellularization protocols of porcine heart valves differ importantly in efficiency of cell removal and susceptibility of the matrix to recellularization with human vascular cells. J Thorac Cardiovasc Surg. 2004; 127(2):399–405. [PubMed: 14762347]
4. Soto-Gutierrez A, Wertheim JA, Ott HC, Gilbert TW. Perspectives on whole-organ assembly: moving toward transplantation on demand. J Clin Invest. 2012; 122(11):3817–3823. [PubMed: 23114604]
5. Ghaedi M, Calle EA, Mendez JJ, Gard AL, Balestrini J, Booth A, et al. Human iPS cell-derived alveolar epithelium repopulates lung extracellular matrix. J Clin Invest. 2013; 123(11):4950–4962. [PubMed: 24135142]
6. Macchiarini P, Jungebluth P, Go T, Asnaghi MA, Rees LE, Cogan TA, et al. Clinical transplantation of a tissue-engineered airway. Lancet. 2008; 372(9655):2023–2030. [PubMed: 19022496]
7. Atala A, Bauer SB, Soker S, Yoo JJ, Retik AB. Tissue-engineered autologous bladders for patients needing cystoplasty. Lancet. 2006; 367(9518):1241–1246. [PubMed: 16631879]
8. Hibino N, McGillicuddy E, Matsumura G, Ichihara Y, Naito Y, Breuer C, et al. Late-term results of tissue-engineered vascular grafts in humans. J Thorac Cardiovasc Surg. 2010; 139(2):431–436. 6 e1–6 e2. [PubMed: 20106404]
9. Guyette JP, Gilpin SE, Charest JM, Tapias LF, Ren X, Ott HC. Perfusion decellularization of whole organs. Nat Protoc. 2014; 9(6):1451–1468. [PubMed: 24874812]
10. Uzarski JS, Xia Y, Belmonte JC, Wertheim JA. New strategies in kidney regeneration and tissue engineering. Current opinion in nephrology and hypertension. 2014; 23(4):399–405. [PubMed: 24848937]
11. Ott HC, Matthiesen TS, Goh SK, Black LD, Kren SM, Netoff TI, et al. Perfusion-decellularized matrix: using nature's platform to engineer a bioartificial heart. Nature medicine. 2008; 14(2):213–221.
12. Ott HC, Clippinger B, Conrad C, Schuetz C, Pomerantseva I, Ikonomou L, et al. Regeneration and orthotopic transplantation of a bioartificial lung. Nature medicine. 2010; 16(8):927–933.
13. Soto-Gutierrez A, Zhang L, Medberry C, Fukumitsu K, Faulk D, Jiang H, et al. A whole-organ regenerative medicine approach for liver replacement. Tissue engineering Part C, Methods. 2011; 17(6):677–686. [PubMed: 21375407]
14. Sullivan DC, Mirmalek-Sani SH, Deegan DB, Baptista PM, Aboushwareb T, Atala A, et al. Decellularization methods of porcine kidneys for whole organ engineering using a high-throughput system. Biomaterials. 2012; 33(31):7756–7764. [PubMed: 22841923]
15. Orlando G, Farney AC, Iskandar SS, Mirmalek-Sani SH, Sullivan DC, Moran E, et al. Production and implantation of renal extracellular matrix scaffolds from porcine kidneys as a platform for renal bioengineering investigations. Ann Surg. 2012; 256(2):363–370. [PubMed: 22691371]
16. Song JJ, Guyette JP, Gilpin SE, Gonzalez G, Vacanti JP, Ott HC. Regeneration and experimental orthotopic transplantation of a bioengineered kidney. Nat Med. 2013; 19(5):646–651. [PubMed: 23584091]
17. Ross EA, Abrahamson DR, St John P, Clapp WL, Williams MJ, Terada N, et al. Mouse stem cells seeded into decellularized rat kidney scaffolds endothelialize and remodel basement membranes. Organogenesis. 2012; 8(2):49–55. [PubMed: 22692231]
18. Ross EA, Williams MJ, Hamazaki T, Terada N, Clapp WL, Adin C, et al. Embryonic stem cells proliferate and differentiate when seeded into kidney scaffolds. J Am Soc Nephrol. 2009; 20(11): 2338–2347. [PubMed: 19729441]

19. Bonandrini B, Figliuzzi M, Papadimou E, Morigi M, Perico N, Casiraghi F, et al. Recellularization of Well-Preserved Acellular Kidney Scaffold Using Embryonic Stem Cells. Tissue Eng Part A. 2014
20. Bijonowski BM, Miller WM, Wertheim JA. Bioreactor design for perfusion-based, highly-vascularized organ regeneration. Current opinion in chemical engineering. 2013; 2(1):32–40. [PubMed: 23542907]
21. Ward HH, Brown-Glaberman U, Wang J, Morita Y, Alper SL, Bedrick EJ, et al. A conserved signal and GTPase complex are required for the ciliary transport of polycystin-1. Molecular biology of the cell. 2011; 22(18):3289–3305. [PubMed: 21775626]
22. Nauli SM, Rossetti S, Kolb RJ, Alenghat FJ, Consugar MB, Harris PC, et al. Loss of polycystin-1 in human cyst-lining epithelia leads to ciliary dysfunction. J Am Soc Nephrol. 2006; 17(4):1015–1025. [PubMed: 16565258]
23. Baptista PM, Siddiqui MM, Lozier G, Rodriguez SR, Atala A, Soker S. The use of whole organ decellularization for the generation of a vascularized liver organoid. Hepatology. 2011; 53(2):604–617. [PubMed: 21274881]
24. Sebinger DD, Ofenbauer A, Gruber P, Malik S, Werner C. ECM modulated early kidney development in embryonic organ culture. Biomaterials. 2013; 34(28):6670–6682. [PubMed: 23773818]
25. Bates CM. Role of fibroblast growth factor receptor signaling in kidney development. American journal of physiology Renal physiology. 2011; 301(2):F245–F251. [PubMed: 21613421]
26. Xia Y, Nivet E, Sancho-Martinez I, Gallegos T, Suzuki K, Okamura D, et al. Directed differentiation of human pluripotent cells to ureteric bud kidney progenitor-like cells. Nat Cell Biol. 2013; 15(12):1507–1515. [PubMed: 24240476]
27. Brown BN, Freund JM, Han L, Rubin JP, Reing JE, Jeffries EM, et al. Comparison of three methods for the derivation of a biologic scaffold composed of adipose tissue extracellular matrix. Tissue Eng Part C Methods. 2011; 17(4):411–421. [PubMed: 21043998]
28. Hoganson DM, Owens GE, O'Doherty EM, Bowley CM, Goldman SM, Harilal DO, et al. Preserved extracellular matrix components and retained biological activity in decellularized porcine mesothelium. Biomaterials. 2010; 31(27):6934–6940. [PubMed: 20584548]
29. Eremina V, Cui S, Gerber H, Ferrara N, Haigh J, Nagy A, et al. Vascular endothelial growth factor a signaling in the podocyte-endothelial compartment is required for mesangial cell migration and survival. J Am Soc Nephrol. 2006; 17(3):724–735. [PubMed: 16436493]
30. Eremina V, Quaggin SE. The role of VEGF-A in glomerular development and function. Current opinion in nephrology and hypertension. 2004; 13(1):9–15. [PubMed: 15090854]
31. Fulco I, Miot S, Haug MD, Barbero A, Wixmerten A, Feliciano S, et al. Engineered autologous cartilage tissue for nasal reconstruction after tumour resection: an observational first-in-human trial. Lancet. 2014
32. Raya-Rivera A, Esquiliano DR, Yoo JJ, Lopez-Bayghen E, Soker S, Atala A. Tissue-engineered autologous urethras for patients who need reconstruction: an observational study. Lancet. 2011; 377(9772):1175–1182. [PubMed: 21388673]
33. Raya-Rivera AM, Esquiliano D, Fierro-Pastrana R, Lopez-Bayghen E, Valencia P, Ordorica-Flores R, et al. Tissue-engineered autologous vaginal organs in patients: a pilot cohort study. Lancet. 2014
34. Wainwright JM, Czajka CA, Patel UB, Freytes DO, Tobita K, Gilbert TW, et al. Preparation of cardiac extracellular matrix from an intact porcine heart. Tissue Eng Part C Methods. 2010; 16(3): 525–532. [PubMed: 19702513]
35. Uygun BE, Soto-Gutierrez A, Yagi H, Izamis ML, Guzzardi MA, Shulman C, et al. Organ reengineering through development of a transplantable recellularized liver graft using decellularized liver matrix. Nature medicine. 2010; 16(7):814–820.
36. Petersen TH, Calle EA, Zhao L, Lee EJ, Gui L, Raredon MB, et al. Tissue-engineered lungs for in vivo implantation. Science (New York, NY). 2010; 329(5991):538–541.
37. Burgkart R, Tron AC, Prodinger P, Culmes M, Tuebel J, van Griensven M, et al. Decellularized kidney matrix for perfused bone engineering. Tissue Eng Part C Methods. 2013

38. Orlando G, Booth C, Wang Z, Totonelli G, Ross CL, Moran E, et al. Discarded human kidneys as a source of ECM scaffold for kidney regeneration technologies. Biomaterials. 2013; 34(24):5915–5925. [PubMed: 23680364]
39. Nakayama KH, Batchelder CA, Lee CI, Tarantal AF. Decellularized rhesus monkey kidney as a three-dimensional scaffold for renal tissue engineering. Tissue engineering Part A. 2010; 16(7): 2207–2216. [PubMed: 20156112]
40. Lotze MT, Deisseroth A, Rubartelli A. Damage associated molecular pattern molecules. Clinical immunology. 2007; 124(1):1–4. [PubMed: 17468050]
41. Bianchi ME. DAMPs, PAMPs and alarmins: all we need to know about danger. J Leukoc Biol. 2007; 81(1):1–5. [PubMed: 17032697]
42. Gilbert TW, Freund JM, Badylak SF. Quantification of DNA in biologic scaffold materials. The Journal of surgical research. 2009; 152(1):135–139. [PubMed: 18619621]
43. Badylak SF, Freytes DO, Gilbert TW. Extracellular matrix as a biological scaffold material: Structure and function. Acta Biomater. 2009; 5(1):1–13. [PubMed: 18938117]
44. Miner JH. Renal basement membrane components. Kidney international. 1999; 56(6):2016–2024. [PubMed: 10594777]
45. Nakayama KH, Lee CC, Batchelder CA, Tarantal AF. Tissue specificity of decellularized rhesus monkey kidney and lung scaffolds. PLoS One. 2013; 8(5):e64134. [PubMed: 23717553]
46. Voytik-Harbin SL, Brightman AO, Kraine MR, Waisner B, Badylak SF. Identification of extractable growth factors from small intestinal submucosa. Journal of cellular biochemistry. 1997; 67(4):478–491. [PubMed: 9383707]
47. O'Brien J, Wilson I, Orton T, Pognan F. Investigation of the Alamar Blue (resazurin) fluorescent dye for the assessment of mammalian cell cytotoxicity. European journal of biochemistry / FEBS. 2000; 267(17):5421–5426. [PubMed: 10951200]

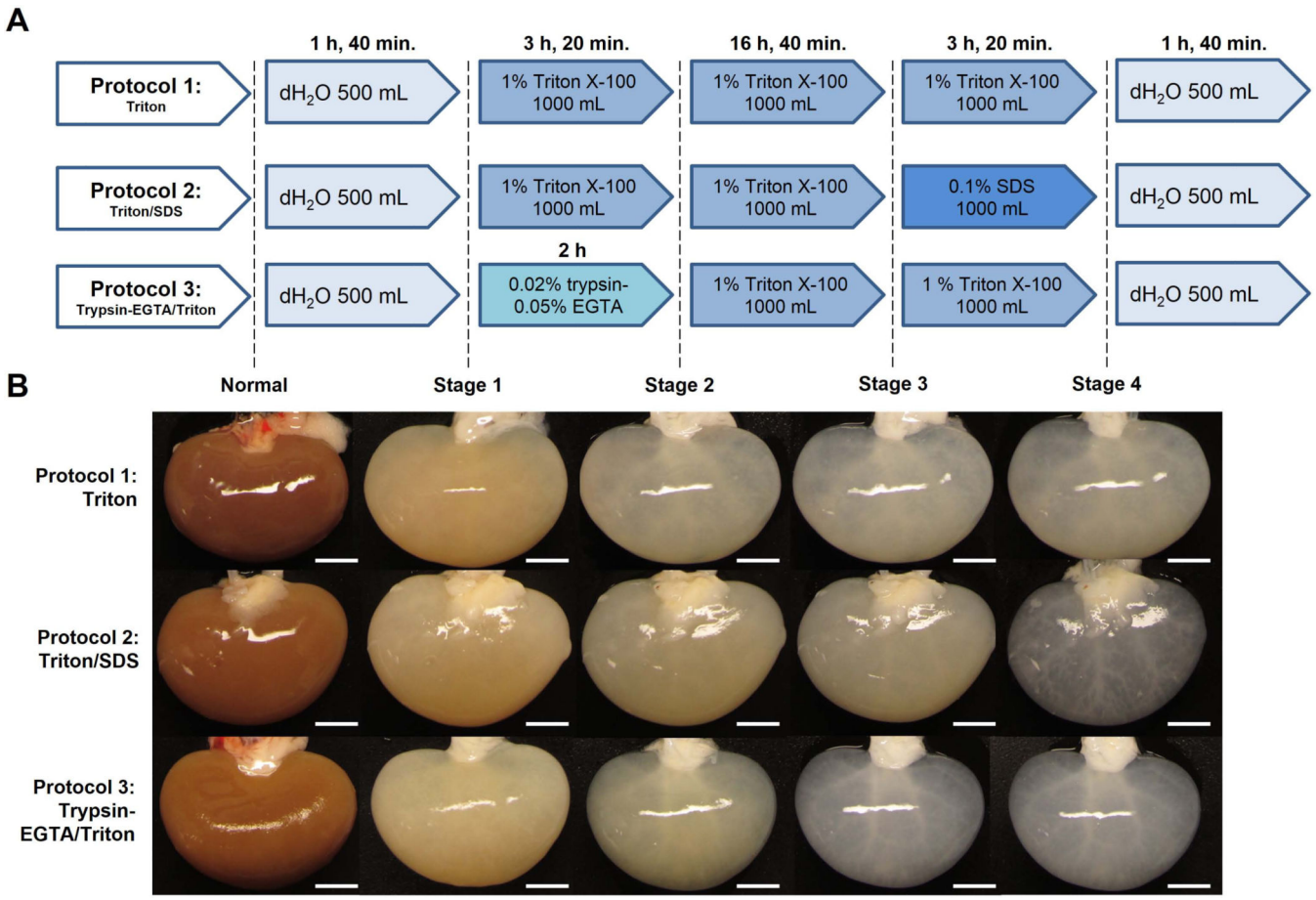

Figure 1. Rat kidney decellularization strategies and macroscopic evaluation of kidney decellularization

(A) Schedules of reagents (quantity and duration) that were sequentially perfused through the renal artery of each rat kidney in three different decellularization protocols: Triton, Triton/SDS, or Trypsin-EGTA/Triton. (B) Representative images of kidneys are shown at each stage throughout the decellularization process as indicated. In the Triton/SDS protocol kidneys became transparent after perfusion of SDS. Using Trypsin-EGTA/Triton, kidneys became progressively transparent early in the decellularization process. Scale bars: 5 mm.

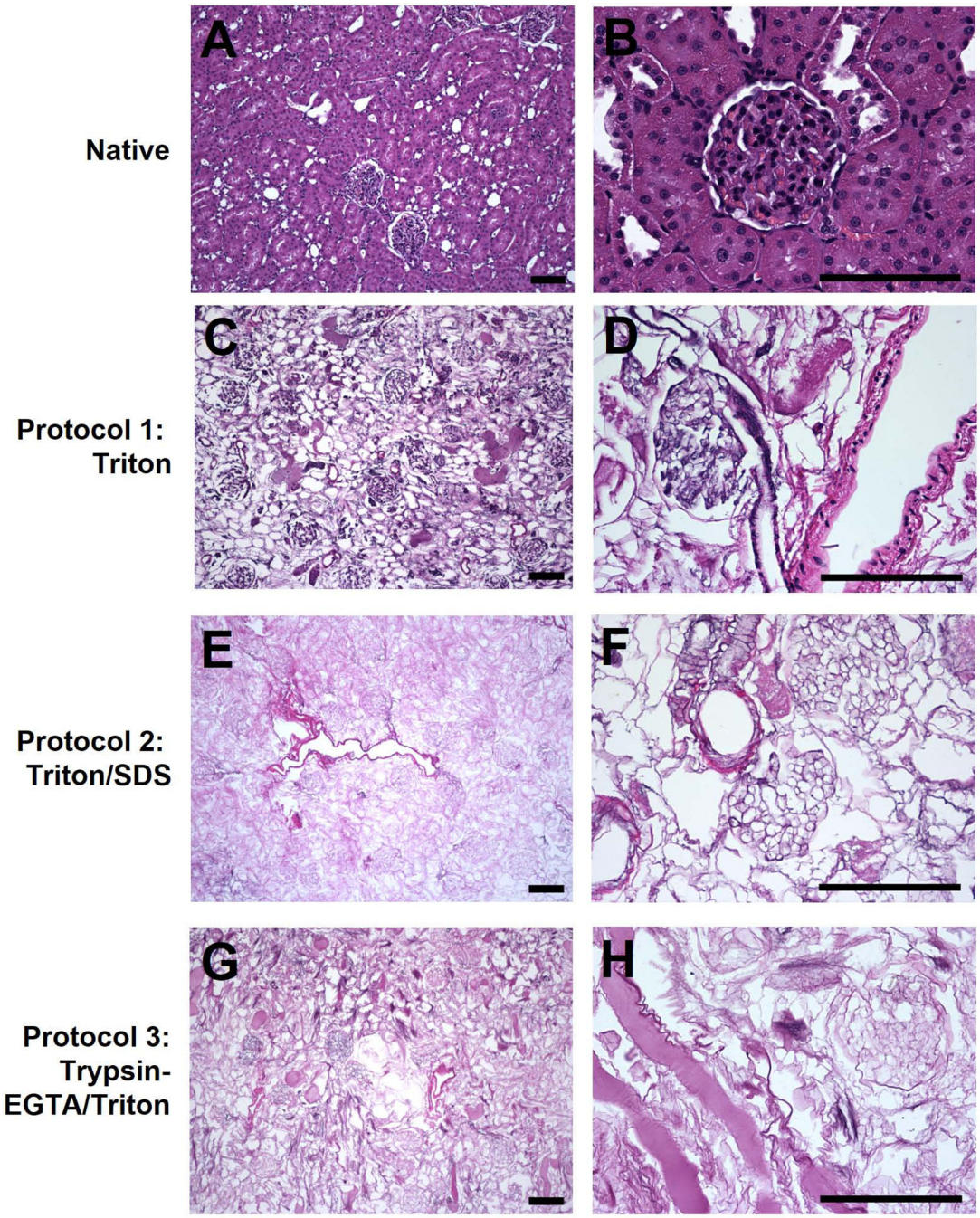

Figure 2. H&E staining of native and decellularized kidneys

Kidneys decellularized using Triton (C–D), Triton/SDS (E–F), or Trypsin-EGTA/Triton (G–H) were stained with H&E and compared to native kidneys (A–B). Decellularization with Triton resulted in retention of endothelial and smooth muscle cells in vessels and mesangial cells within the glomerulus. Triton/SDS and Trypsin-EGTA/Triton removed all cells as assessed by H&E. Representative images are shown at 10× (A, C, E, G) and 40× (B, D, F, H) magnification. Scale bars: 50 μm.

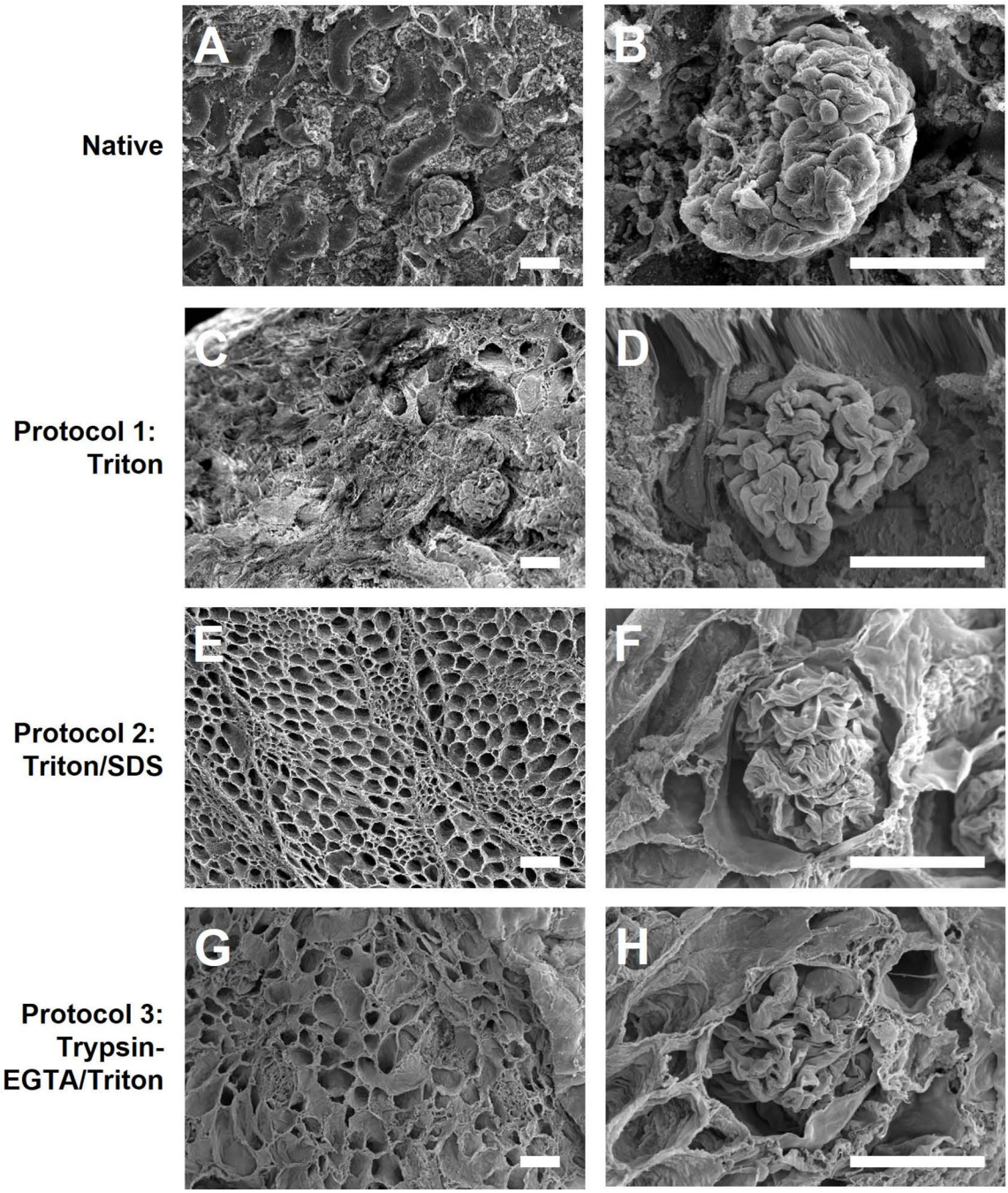

Figure 3. Scanning electron micrographs of native and decellularized kidneys

Kidneys decellularized using Triton (C–D), Triton/SDS (E–F), or Trypsin-EGTA/Triton (G–H) were imaged using scanning electron microscopy and compared to native kidneys (A–B). Representative images are shown at 250× (A, C, E, G) and 850× (B, D, F, H) magnification. Decellularization with Triton/SDS or Trypsin-EDTA/Triton removed parenchyma cells resulting in a honeycomb appearance of the renal ECM (E, G) and preservation of glomerular structures (F, H) which are a benchmark for renal decellularization. Scale bars: 50 μm.

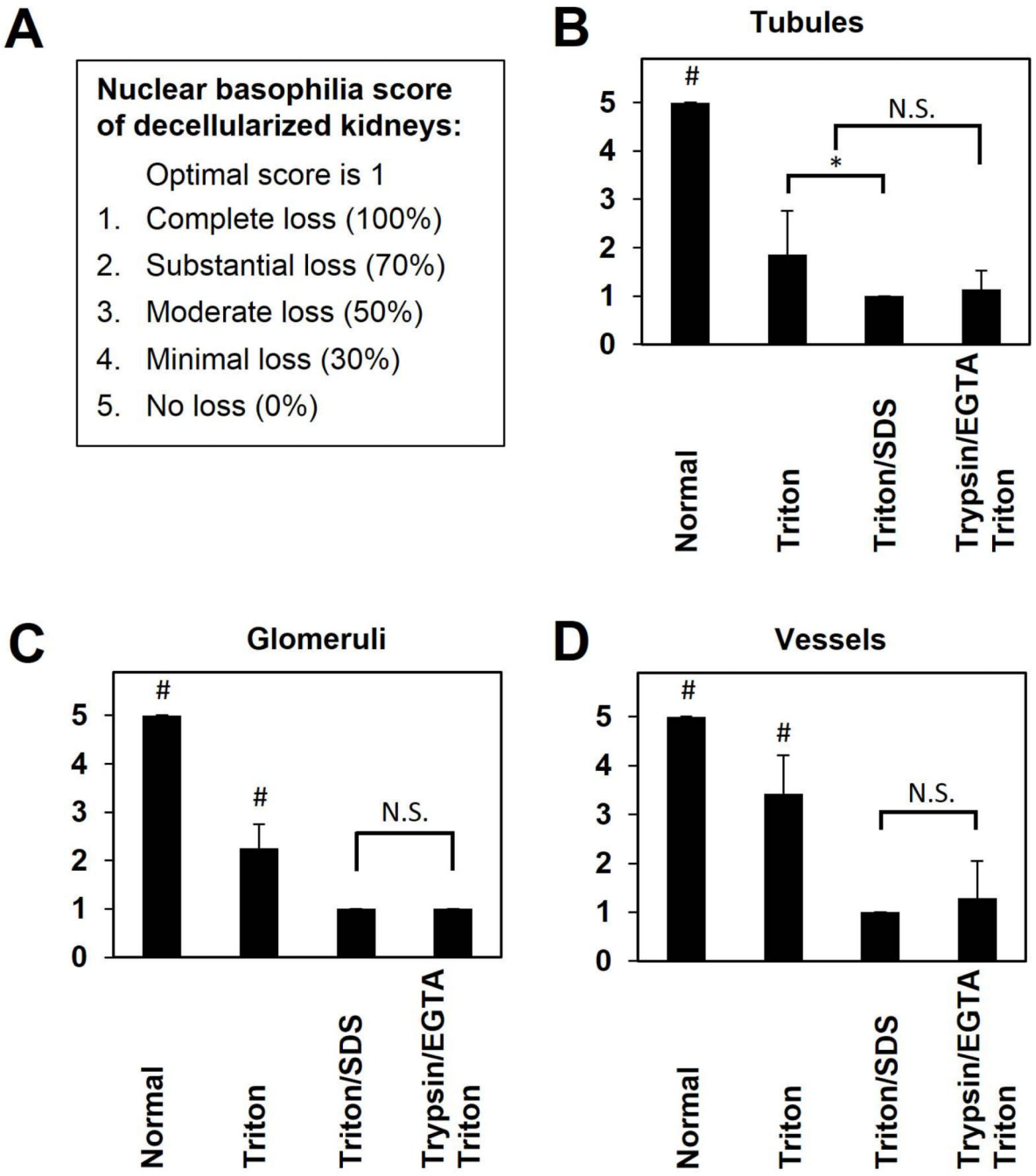

Figure 4. Nuclear basophilia score of decellularized kidneys

This scoring system assesses the removal of cells (loss of nuclear basophilia) from components of the decellularized kidney ECM as evaluated by a pathologist blinded to each protocol used. A score of 1 is optimal. 1- Complete (100%) removal of cells; 2- Substantial (70%) loss; 3- Moderate (50%) loss; 4- Minimal (30%) loss; 5- No (0%) loss. Results are presented as mean ± standard deviation. # indicates a significant difference in means compared with all other groups ($p<0.05$), * indicates a significant difference in means

between conditions specified by horizontal and vertical bars ($p<0.05$), and N.S. indicates no significant difference in means as specified.

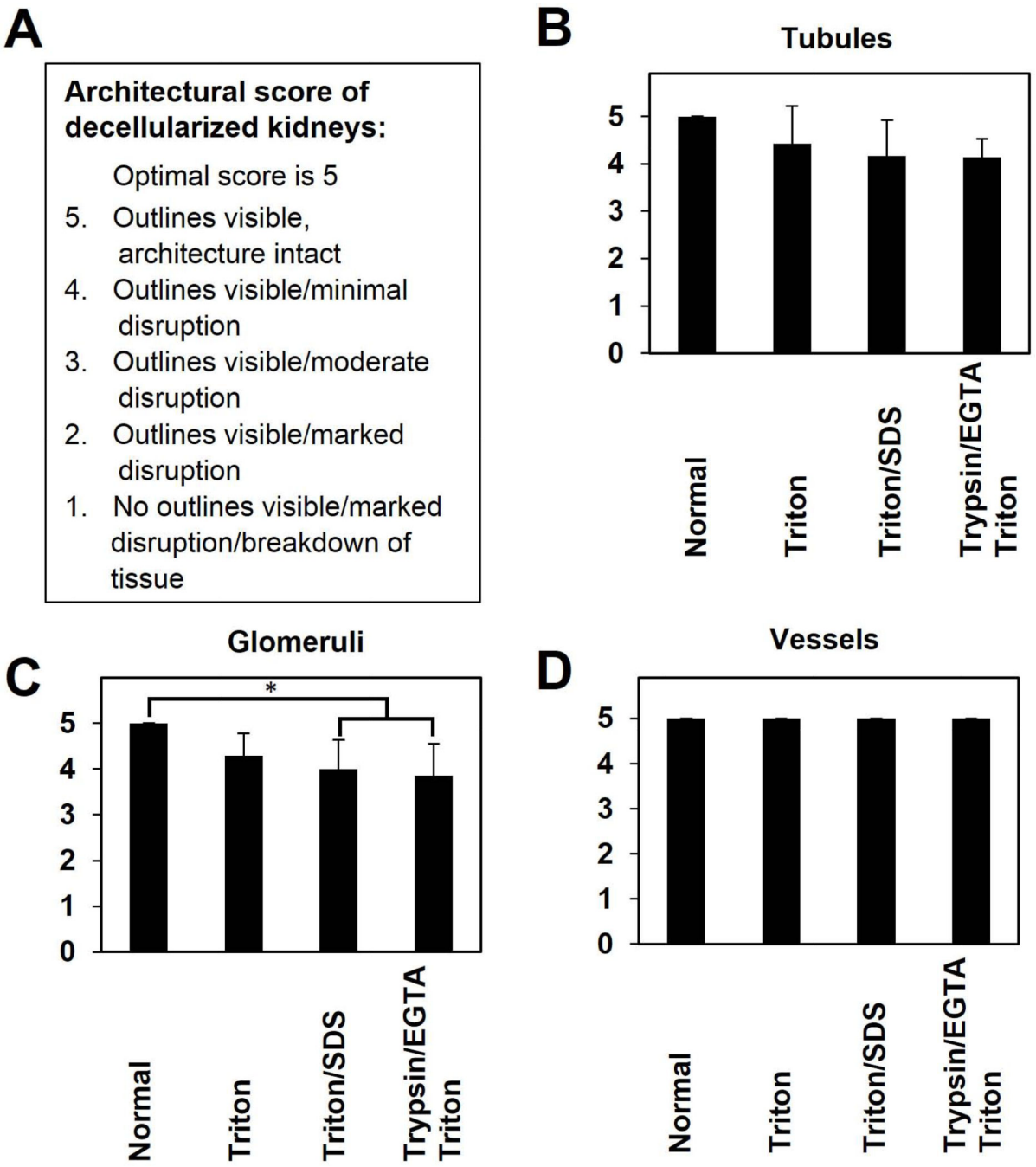

Figure 5. Architectural score of decellularized kidneys

This scoring system evaluates retention of microscopic ECM components evaluated by a pathologist blinded to each protocol used. A score of 5 is optimal. 5-Outlines visible, architecture intact; 4-Outlines visible/Minimal disruption; 3-Outlines visible/Moderate disruption; 2-Outlines visible/marked disruption; 1-No outlines visible/marked disruption/ breakdown of tissue. Results are presented as mean ± standard deviation. * indicates a significant difference in means between the conditions specified by the horizontal and vertical bars ($p<0.05$).

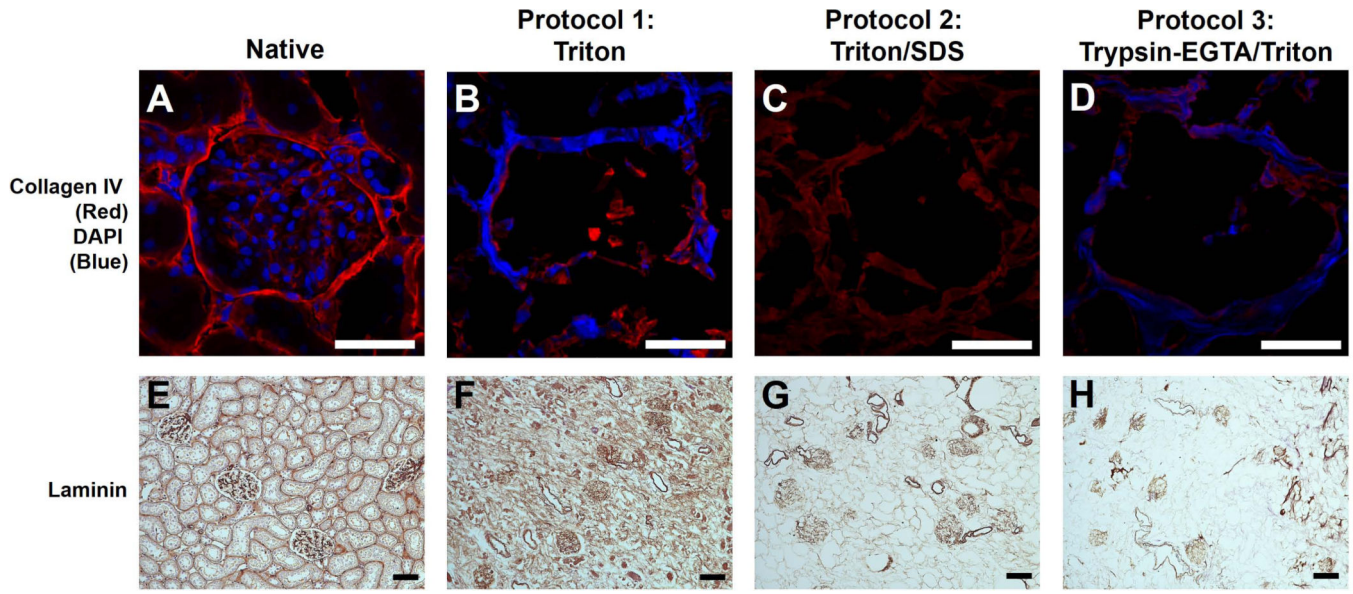

Figure 6. Collagen IV and laminin staining of normal and decellularized kidneys using three decellularization strategies

Native kidneys (A, E) or kidneys decellularized using Triton (B, F), Triton/SDS (C, G), or Trypsin-EGTA/Triton (D, H) were stained for collagen IV/cell nuclei (top row) or laminin (bottom row). Collagen IV (red, top row) is retained in the glomeruli (pictured) and other structures (e.g., renal capsule and tubules, not shown) in all protocols though there was some qualitative loss of protein. Only Triton/SDS caused complete loss of nuclei as seen by the absence of DAPI staining (blue). Trypsin-EGTA/Triton yielded DNA debris within the matrix, as evidenced by residual DAPI staining. Laminin (bottom row) was retained to a degree in each protocol. In Triton/SDS and Trypsin-EGTA/Triton decellularized kidneys, laminin was mostly found within the glomeruli and, to a lesser extent, tubules. Representative images are shown at 40× magnification for collagen IV (top row, 25 μm scale bars) and 10× magnification for laminin (bottom row, 50 μm scale bars).

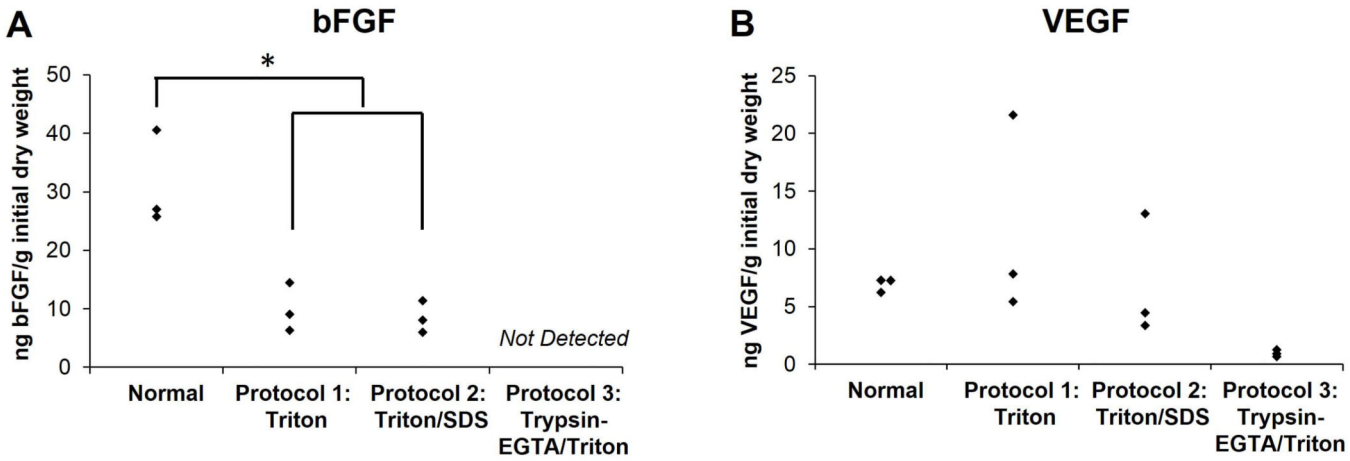

Figure 7. Evaluation of growth factor retention in normal and decellularized kidneys

Normal kidneys or kidneys decellularized using Triton, Triton/SDS, or Trypsin-EGTA/Triton were lyophilized, digested enzymatically and analyzed for bFGF (A) or VEGF (B) content using ELISA. Growth factor retention was normalized by initial dry weight of native, control kidneys for comparison across all protocols. Results are presented as minimum, median, and maximum values (n=3 kidneys per group). Asterisks indicate significant differences in means as specified ($p<0.05$). No significant differences were found in retention of VEGF.

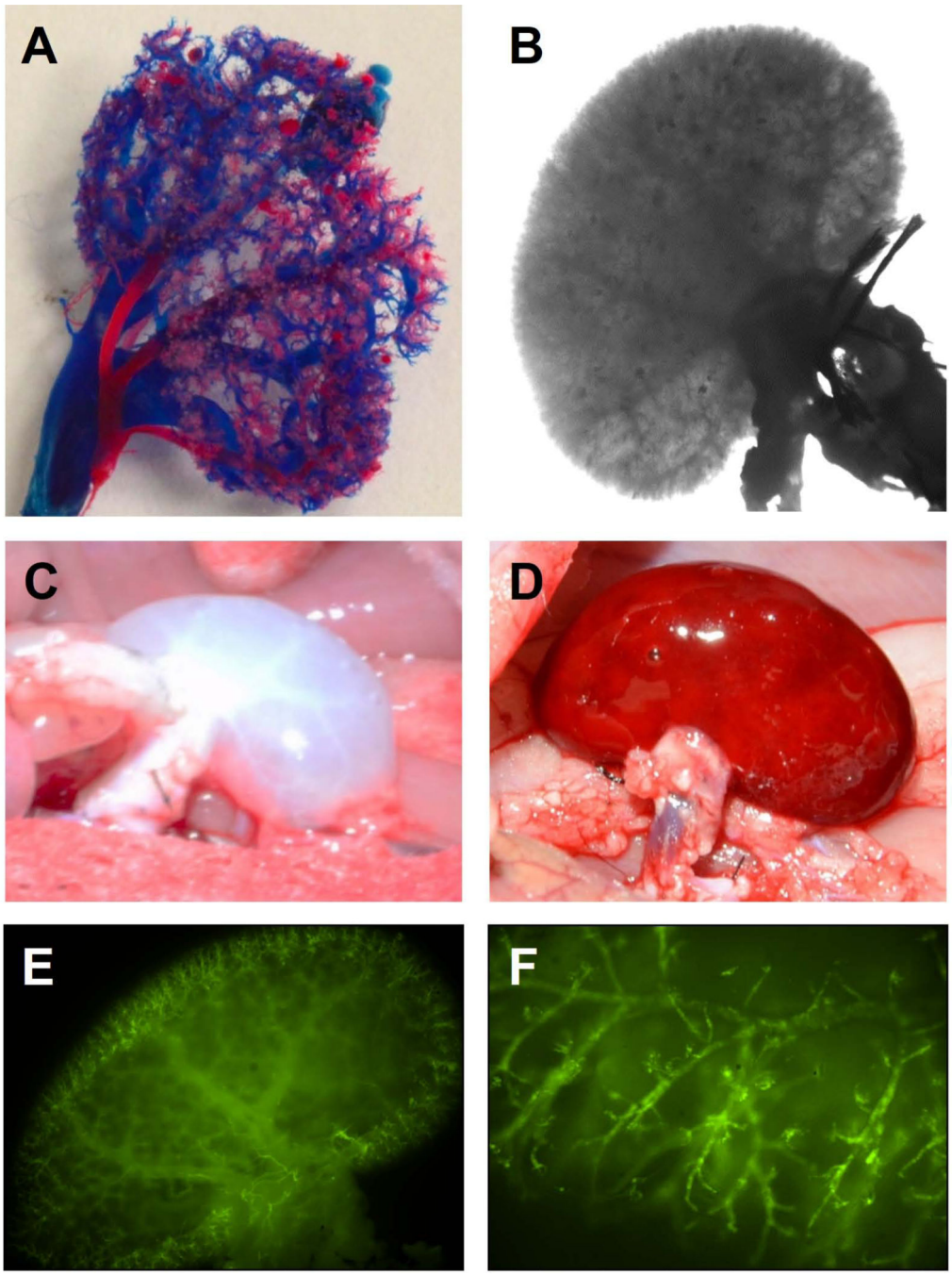

Figure 8. Analysis of vasculature, transplantation, and endothelialization of decellularized rodent kidneys

Corrosion casting was used to assess the integrity of the vasculature in Triton/SDS-decellularized kidneys. An intact vasculature is illustrated by polymers injected through the renal artery (red) and vein (blue) (A) and by bright-field microscopy (B). Gross aspect of transplanted Triton/SDS-decellularized kidney before (C) and after (D) 30 minutes of reperfusion of blood within Sprague-Dawley recipient rat. Human iPSC-derived endothelial cells, labeled with CFSE (green) were injected through the renal artery. Fluorescence

microscopy shows incorporation of cells into vascular structures, which were well distributed throughout the kidney (E, F).

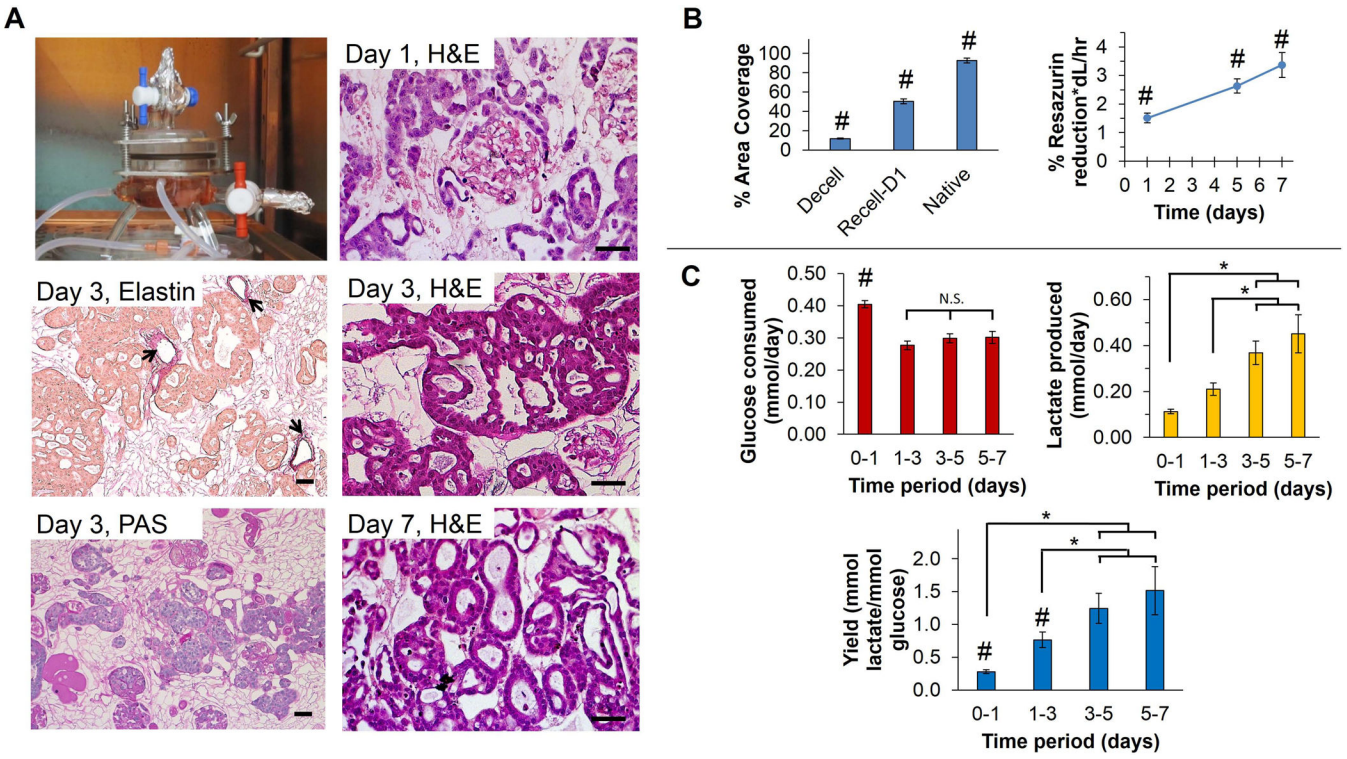

Figure 9. Recellularization of whole-kidney decellularized ECM scaffolds with tubular epithelial cells

(A) Human RCTE cells were infused into Triton/SDS-decellularized kidneys through the renal artery and cultured within a perfusion bioreactor. Representative images of kidney sections stained with H&E at days 1, 3, and 7, and elastin and PAS at day 3 are shown. Weigert's resorcin-fuchsin (WRF) staining of elastin demonstrates retention of arteriolar structure and indicates that although RCTE cells were infused through the renal artery they did not remain in this location (arrows depict elastin staining). PAS stain indicates retention of the basement membrane depicted in dark pink, indicating that RCTE cells resided on the basement membrane and formed what appear to be tubular structures. Scale bars: 50 μm. (B) % Area coverage was quantified using ImageJ and decellularized (Decell) and recellularized (Recell-D1) kidneys were compared to native, untreated kidneys. The renal ECM makes up 12.0±0.5% of the total area of decellularized kidneys while normal kidneys have cells and ECM covering 92.7±2.6% with the remaining ~7% taken up by intraluminal (vascular and tubule) open space. Renal cells and adjacent ECM occupied ~50% of the surface area of recellularized kidneys at day 1 as determined in 5 high-powered fields each at 3 separate levels inside the 3D scaffold (15 fields total per kidney). Resazurin reduction assay revealed a significant increase in RCTE metabolic activity over time ($p<0.05$). (C) Glucose consumption declined after day 1, and remained stable through day 7. Lactate production steadily increased; however, indicating a shift toward glycolytic metabolism. # indicates a significant difference in means compared with all other groups ($p<0.05$), * indicates a significant difference in means between conditions specified by horizontal and vertical bars ($p<0.05$), and N.S. indicates no significant difference in means as specified.

Am J Transplant. Author manuscript; available in PMC 2016 January 01.

Table 1

Summary Evaluation of Decellularization Protocols

Selection criteria	**Protocol 1: Triton**		**Protocol 2: Triton/SDS**		**Protocol 3: Trypsin-EGTA/Triton**	
Macroscopic appearance (transparency of gross tissue is the goal)	−		+		+	
Microscopic appearance (H&E, SEM, cell removal, maintenance of architecture is goal)	−		+		+/−	
DNA reduction (goal: >95%)	−		+		−	
Nuclear basophilia score (goal score is 1.0–2.0)	−	Glomeruli: 2.1±0.4 Tubules: 1.9±0.9 Vessels: 3.4±0.8	+	Glomeruli: 1.0±0.0 Tubules: 1.0±0.0 Vessels: 1.0±0.0	+	Glomeruli: 1.1±0.4 Tubules: 1.1±0.4 Vessels: 1.3±0.8
Architectural score (goal score is 4.0–5.0)	+	Glomeruli: 4.3±0.5 Tubules: 4.4±0.8 Vessels: 5.0±0.0	+	Glomeruli: 4.0±0.6 Tubules: 4.2±0.8 Vessels: 5.0±0.0	+	Glomeruli: 3.9±0.7 Tubules: 4.1±0.4 Vessels: 5.0±0.0
ECM (collagen, laminin) retention (goal is retention of proteins)	+		+/−		+/−	
Growth factor (bFGF, VEGF) retention (goal: >30% retention)	+		+		−	

For each criterion, protocols were evaluated and assigned one of three values: good (+), fair (+/−), or poor (−) at reaching a target goal. Each protocol was evaluated independently of the other two protocols, and is compared to normal kidneys.